An Improved Calibration of the Wavelength Dependence of Metallicity on the Cepheid Leavitt Law

Louise Breuval, Adam G. Riess, Pierre Kervella, Richard I. Anderson, Martino Romaniello

The Astrophysical Journal, 939:89 (17pp), 2022 November 10 https://doi.org/10.3847/1538-4357/ac97e2

An Improved Calibration of the Wavelength Dependence of Metallicity on the Cepheid Leavitt Law

Louise Breuval[1,2], Adam G. Riess[1,3], Pierre Kervella[2], Richard I. Anderson[4], and Martino Romaniello[5]
[1] Department of Physics and Astronomy, Johns Hopkins University, Baltimore, MD 21218, USA; lbreuva1@jhu.edu
[2] LESIA, Observatoire de Paris, Université PSL, CNRS, Sorbonne Université, Université Paris Cité, 5 place Jules Janssen, F-92195 Meudon, France
[3] Space Telescope Science Institute, 3700 San Martin Drive, Baltimore, MD 21218, USA
[4] Institute of Physics, Laboratory of Astrophysics, École Polytechnique Fédérale de Lausanne (EPFL), Observatoire de Sauverny, 1290 Versoix, Switzerland
[5] European Southern Observatory, Karl-Schwarzschild-Strasse 2, D-85478 Garching bei München, Germany
Received 2022 May 11; revised 2022 September 15; accepted 2022 October 4; published 2022 November 9

Abstract

The Cepheid period–luminosity (PL) relation (or Leavitt law) has served as the first rung of the most widely used extragalactic distance ladder and is central to the determination of the local value of the Hubble constant (H_0). We investigate the influence of metallicity on Cepheid brightness, a term that significantly improves the overall fit of the distance ladder, to better define its wavelength dependence. To this aim, we compare the PL relations obtained for three Cepheid samples having distinct chemical composition (in the Milky Way and Magellanic Clouds) and focusing on the use of improved and recent data while covering a metallicity range of about 1 dex. We estimate the metallicity effect (hereafter γ) in 15 filters from mid-IR to optical wavelengths, including five Wesenheit indices, and we derive a significant metallicity term in all filters, in agreement with recent empirical studies and models, in the sense of metal-rich Cepheids being brighter than metal-poor ones. We describe the contribution of various systematic effects in the determination of the γ term. We find no evidence of γ changing over the wavelength range 0.5–4.5 μm, indicating that the main influence of metallicity on Cepheids is in their luminosity rather than color. Finally, we identify factors that sharpen the empirical constraints on the metallicity term over past studies, including corrections for the depth of the Magellanic Clouds, better-calibrated Cepheid photometry, improved Milky Way extinction estimates, and revised and expanded metallicity measurements in the LMC.

Unified Astronomy Thesaurus concepts: Cepheid distance (217); Hubble constant (758); Metallicity (1031)

1. Introduction

The Cepheid period–luminosity (PL) relation (or Leavitt law; Leavitt & Pickering 1912) is a fundamental tool for measuring astronomical distances and has been used for decades to estimate the current expansion rate of the universe, the Hubble constant (Freedman et al. 2001; Riess et al. 2022). Recently, a significant tension of 5σ has arisen between the prediction of H_0 from the cosmic microwave background data from Planck Collaboration et al. (2020) assuming a ΛCDM model, $H_0 = 67.4 \pm 0.5\,\mathrm{km\,s^{-1}\,Mpc^{-1}}$, and its empirical estimate based on Cepheids and Type Ia supernova (SN Ia) measurements, $H_0 = 73.04 \pm 1.04\,\mathrm{km\,s^{-1}\,Mpc^{-1}}$ (Riess et al. 2022). The persistence of this discrepancy could have significant implications in cosmology, as it may suggest a breach in the standard model (Di Valentino et al. 2021). It is therefore important to empirically scrutinize the nature of the Leavitt law.

In the present paper, we aim at measuring the influence of chemical abundance on Cepheid brightness, as this term has been found to significantly improve the quality of the fit of the distance ladder. The difference in metallicity between Cepheids used to calibrate the PL relation and Cepheids in SN Ia host galaxies is usually taken into account by including a corrective term (γ) in the PL relation, such that

$$M = \alpha\,(\log P - \log P_0) + \delta + \gamma\,[\mathrm{Fe/H}]. \quad (1)$$

The majority of extragalactic Cepheids in SN Ia hosts have inferred abundances that are similar to those in two distance ladder anchors, the Milky Way (MW) and NGC 4258, in terms of metal content (see Figure 21 in Riess et al. 2022). However, the Large Magellanic Cloud (LMC), which contains more metal-poor Cepheids, is also often used as an anchor in the distance ladder (Riess et al. 2019); its distance was measured with high precision by Pietrzyński et al. (2019) using detached eclipsing binaries (DEBs). The improved characterization of the distance ladder depends on an improved constraint on the metallicity term to span such a range of metallicity. The best accuracy on this term can thus be obtained by using an even larger metallicity range including the even more metal-poor Small Magellanic Cloud (SMC) and its recently measured DEB distance (Graczyk et al. 2020).

Various estimates of the metallicity effect were published in the last two decades based on different methods, samples, photometry, distances, or chemical abundances. They are listed in Table 1. Early studies using nonlinear convecting models (Bono et al. 1999, 2008; Caputo et al. 2000; Marconi et al. 2005) based on masses and luminosities provided by stellar evolutionary calculations predicted a positive metallicity effect ($\gamma > 0$), meaning that metal-rich Cepheids are fainter than metal-poor ones. A positive metallicity term might be explained as a strictly atmospheric effect from line blanketing with higher metallicity producing more absorption lines to decrease the flux emitted by the star and make it appear fainter than expected in the optical (Freedman & Madore 2011), although this explanation does not address possible changes to a Cepheid's bolometric luminosity. More recently, Anderson et al. (2016) used stellar

Table 1
Empirical and Theoretical Estimates of the Metallicity Effect (γ in mag dex^{-1}) on Cepheid Brightness

Band	γ	Reference	Method	
		Theoretical Studies		
V	$+0.40$	Bono et al. (1999)	Nonlinear convecting models	[Fe/H]
K	-0.08			
V, I	$+0.27$	Caputo et al. (2000)	Nonlinear convecting models	[Fe/H]
V, I	$\gamma > 0$	Marconi et al. (2005)	Nonlinear convecting models	[Fe/H]
W_{VI}	$+0.05 \pm 0.03$	Bono et al. (2008)	Nonlinear convecting models	[Fe/H]
V	-0.277 ± 0.102	Anderson et al. (2016)	Geneva evolution models including the effects of rotation (second crossing), average between blue and red edge	
H	-0.214 ± 0.086			
W_{VI}	-0.221 ± 0.097			
W_H	-0.205 ± 0.084			
W_G	-0.13 to -0.25	De Somma et al. (2022)	Nonlinear convecting models	
W_H	-0.13 to -0.19			
W_{VI}	-0.15 to -0.17			
W_{VK}	-0.14 to -0.18			
		Empirical Studies		
W_{VI}	-0.24 ± 0.16	Kennicutt & Stetson (1998)	Two fields in M101	[O/H]
W_{VI}	-0.24 ± 0.05	Sakai et al. (2004)	TRGB/Cepheid distances to nearby galaxies	[O/H]
W_{VI}	-0.29 ± 0.10	Macri et al. (2006)	Two fields in NGC 4258	[O/H]
K	~ 0	Romaniello et al. (2008)	MW, LMC, SMC + HR spectra	[Fe/H]
V	$\gamma > 0$			
W_H	-0.23 ± 0.17	Riess et al. (2009)	HST photometry, NGC 4258	[O/H]
W_{VI}	-0.29 ± 0.11	Scowcroft et al. (2009)	Four fields in M33	[O/H]
W_H	-0.10 ± 0.09	Riess et al. (2011)	HST photometry, MW, LMC, NGC 4258	[O/H]
V	$+0.50 \pm 0.31$	Freedman & Madore (2011)	Abundances of individual LMC Cepheids	[Fe/H]
J	$+0.14 \pm 0.07$			
H	$+0.05 \pm 0.02$			
K	$+0.02 \pm 0.03$			
[3.6 μm]	-0.39 ± 0.16			
[4.5 μm]	-0.25 ± 0.18			
[5.8 μm]	-0.39 ± 0.17			
[8.0 μm]	-0.38 ± 0.16			
(3.6 μm)	-0.09 ± 0.29	Freedman et al. (2011)	MW, LMC, SMC	[Fe/H]
V	$+0.09 \pm 0.10$	Storm et al. (2011a)	MW, LMC, SMC + IRSB BW distances $p = 1.55 - 0.186 \log P$ (Storm et al. 2011b)	[Fe/H]
I	-0.06 ± 0.10			
W_{VI}	-0.23 ± 0.10			
J	-0.10 ± 0.10			
K	-0.11 ± 0.10			
W_{JK}	-0.10 ± 0.10			
V	$+0.23 \pm 0.11$	Groenewegen (2013)	MW, LMC, SMC + IRSB BW distances $p = 1.50 - 0.24 \log P$	[Fe/H]
K	-0.05 ± 0.10			
W_{VK}	$+0.04 \pm 0.10$			
W_H	-0.14 ± 0.06	Riess et al. (2016)	HST photometry, MW, LMC, NGC 4258	[O/H]
V	-0.022 ± 0.076	Wielgórski et al. (2017)	LMC, SMC + DEB distances	[Fe/H]
I	-0.015 ± 0.071			
J	-0.042 ± 0.069			
H	-0.012 ± 0.069			
K	-0.017 ± 0.069			
W_{VI}	-0.025 ± 0.067			
W_{JK}	-0.022 ± 0.067			
V	-0.238 ± 0.186	Gieren et al. (2018)	MW, LMC, SMC + IRSB BW distances	[Fe/H]

Table 1
(Continued)

Band	γ	Reference	Method	
I	-0.293 ± 0.150		$p = 1.55 - 0.186 \log P$ (Storm et al. 2011b)	
W_{VI}	-0.335 ± 0.059			
J	-0.270 ± 0.108			
K	-0.232 ± 0.064			
W_{JK}	-0.221 ± 0.053			
V	-0.041 ± 0.260	Groenewegen (2018)	MW Gaia DR2 parallaxes, ZP $= -0.046$ mas	[Fe/H]
K	-0.168 ± 0.146			
W_{VK}	-0.188 ± 0.142			
W_H	-0.17 ± 0.06	Riess et al. (2019)	HST photometry, MW, LMC, NGC 4258	[O/H]
K	-0.082 ± 0.138	Ripepi et al. (2020)	MW Gaia DR2 parallaxes, ZP $= -0.049$ mas	[Fe/H]
W_{JK}	-0.284 ± 0.115			
K	-0.456 ± 0.099	Ripepi et al. (2021)	MW Gaia EDR3 parallaxes + HR spectra	[Fe/H]
W_{JK}	-0.465 ± 0.071			
W_{VK}	-0.459 ± 0.107			
V	-0.048 ± 0.055	Breuval et al. (2021)	MW, LMC, SMC	[Fe/H]
I	-0.138 ± 0.053		Gaia EDR3 parallaxes + DEB distances	
W_{VI}	-0.251 ± 0.057			
J	-0.208 ± 0.052			
H	-0.152 ± 0.092			
K	-0.221 ± 0.051			
W_{JK}	-0.214 ± 0.057			
W_H	-0.217 ± 0.046	Riess et al. (2022)	Cepheids with HST/WFC3 photometry	[O/H]
W_G	-0.520 ± 0.090	Ripepi et al. (2022a)	MW Gaia EDR3 parallaxes + HR spectra	[Fe/H]

models from the Geneva group including the effects of rotation and derived a strong negative dependence in the optical and near-infrared (NIR; see Section 5.5), meaning that metal-rich Cepheids would be brighter (see also De Somma et al. 2022).

On the other hand, almost all recent empirical studies have obtained a negative metallicity term ($\gamma < 0$) based on extragalatic Cepheids (Macri et al. 2006; Scowcroft et al. 2009), Baade–Wesselink distances of MW and Magellanic Cloud Cepheids (Storm et al. 2011a; Groenewegen 2013; Gieren et al. 2018), DEB distances for Magellanic Cloud Cepheids (Wielgórski et al. 2017), and Gaia (Gaia Collaboration et al. 2016) DR2 or EDR3 parallaxes (Groenewegen 2018; Ripepi et al. 2020; Riess et al. 2021; Ripepi et al. 2021, 2022a). Romaniello et al. (2008) provided a range of metal abundances of individual LMC Cepheids that were used by Freedman & Madore (2011) to derive a negative metallicity term in the mid-infrared (MIR) Spitzer bands, becoming progressively weaker and then positive toward optical wavelengths, with a crossover around the NIR. However, a significant revision, as well as an expansion, of these measurements by Romaniello et al. (2022) concluded that there were no significant differences among the individual metallicities of LMC Cepheids, negating the ability to constrain the metallicity term internal to the LMC. The nontrivial depth of the Magellanic Clouds is also an important factor, as the scale of the metallicity term between the Clouds and the MW is <0.1 mag.

Improving data quality necessitates a study of the metallicity term outside the context of the distance ladder and over a broader range of wavelengths. Because the accuracy required to resolve the metallicity term, a few hundredths of a magnitude, is comparable to historic zero-point errors, consistent calibration of Cepheid photometry is paramount. While the distance ladder combines constraints on the metallicity term from both metallicity gradients within hosts and abundance differences between hosts (Riess et al. 2022), we focus here on the constraints from the latter, as these offer the best combination of simplicity, wavelength coverage, and constraining power.

In Breuval et al. (2021, hereafter B21), we calibrated γ in seven ground-based filters covering NIR and optical wavelengths, including two Wesenheit indices. The present work aims at improving, expanding, and complementing this preliminary study with new data, in particular by including two additional MIR Spitzer bands, three additional optical Gaia bands, and three supplementary Wesenheit indices (including the Hubble Space Telescope, HST, reddening-free W_H band used in the SH0ES papers; e.g., Riess et al. 2022), resulting in a total of 15 different filters. The large wavelength coverage ($0.5\ \mu\text{m} < \lambda < 4.5\ \mu\text{m}$) also allows for the study of a possible dependence between γ and λ. Following B21, we adopt three Cepheid samples of different chemical abundances that also have precise distances: MW, LMC, and SMC Cepheids. Section 2 describes the data used in this analysis. The method is outlined in Section 3, and the results are given in Section 4. We discuss our findings in Section 5 and conclude with perspectives in Section 6.

2. Data

This section describes the catalogs used in this analysis (photometry, reddenings, distances, and metallicities); they are listed in Table 2.

Table 2
References for the Data Adopted in This Study

	MW	LMC	SMC
V, *I*	Berdnikov (2008)	Soszyński et al. (2015) Ulaczyk et al. (2013)	Soszyński et al. (2015)
J, *H*, *K*	Monson & Pierce (2011)	*J*, *K*: Ripepi et al. (2022b) *H*: Macri et al. (2015), Persson et al. (2004)	*J*, *K*: Ripepi et al. (2017) *H*: Kato et al. (2007)
G, BP, RP	Gaia DR3 (Ripepi et al. 2022c)	Gaia DR3 (Ripepi et al. 2022c)	Gaia DR3 (Ripepi et al. 2022c)
[3.6 μm], [4.5 μm]	Monson et al. (2012)	Scowcroft et al. (2011)	Scowcroft et al. (2016)
F160W, F555W, F814W	Riess et al. (2021)	Riess et al. (2019)	⋯
Reddening	(a) Bayestar dust map (Green et al. 2019) (b) Period–color relation (Riess et al. 2022) (c) SPIPS method (Trahin et al. 2021)	Skowron et al. (2021) reddening maps	Skowron et al. (2021) reddening maps
Distance	Bailer-Jones et al. (2021) distances (includes ZP correction by Lindegren et al. 2021) + additional ZP of 0.014 mas (Riess et al. 2021)	DEB distance $49.59 \pm 0.09 \pm 0.54$ kpc (Pietrzyński et al. 2019) + geometry correction	DEB distance $62.44 \pm 0.47 \pm 0.81$ kpc (Graczyk et al. 2020) + geometry correction
Metallicity	Genovali et al. (2014, 2015) [Fe/H] = +0.088 dex ($\sigma = 0.022$) (depends on the sample)	Romaniello et al. (2022) [Fe/H] = -0.407 ± 0.020 dex	Gieren et al. (2018) [Fe/H] = -0.75 ± 0.05 dex

2.1. Photometry

In order to minimize the systematic uncertainties related to the use of the disparate photometric systems present in many literature compilations of Cepheid magnitudes, we adopt the most homogeneous and consistently calibrated data sets available, while ensuring at the same time that the best light-curve coverage is obtained for the Cepheids.

NIR ground J, H, and K filters. In the NIR, we adopted the photometry from Monson & Pierce (2011) transformed in the Two Micron All Sky Survey (2MASS) system for MW Cepheids. Mean magnitudes of LMC Cepheids are taken from the VISTA survey for the Magellanic Clouds (VMC) by Ripepi et al. (2022b) in *J* and *K* and the Synoptic Survey by Macri et al. (2015, hereafter M15) in *H*; the latter also includes additional Cepheids from Persson et al. (2004). Finally, the VMC survey by Ripepi et al. (2017) provides *J*- and *K*-band light curves for a large number of SMC Cepheids. We complemented these data with the *H*-band single-epoch photometry from the Kato et al. (2007) Point Source Survey. In the LMC and SMC, VMC mean magnitudes are converted into the 2MASS system using the transformations from González-Fernández et al. (2018). Finally, empirically derived transformations for zero-points and color terms are applied to LMC and SMC NIR photometry to match the 2MASS system; the details can be found in Sections 2.2 and 2.3 in B21.

Optical ground V and I filters. In the *V* and *I* bands, we adopt the compilation of light curves from Berdnikov (2008) for MW Cepheids. In the LMC and SMC, we adopt the OGLE-IV survey from Soszyński et al. (2015), combined with the Shallow Survey of bright LMC Cepheids by Ulaczyk et al. (2013). For consistency, we select the list of Cepheids from Macri et al. (2015) for the LMC sample. We note the lack of a more consistently calibrated, modern set of all-sky optical Cepheid data for the MW sample, making it the most limiting data set in the following studies.

Gaia optical G, BP, and RP filters. We used the intensity-averaged mean magnitudes provided in the Gaia DR3 "vari_Cepheid" catalog by Ripepi et al. (2022c) in the three optical Gaia bands for MW, LMC, and SMC Cepheids. For the LMC and SMC samples, we adopted all Cepheids in the regions defined in Table 1 by Ripepi et al. (2022c). As for MW Cepheids, we considered that "AllSky" Cepheids are those outside of the regions of the LMC, SMC, M31, and M33 (Ripepi et al. 2022c). These mean magnitudes are internally photometrically consistent. All stars have at least 15 epochs in the Gaia bands and an average of 45 epochs.

Spitzer MIR [3.6 μm] and [4.5 μm] filters. A sample of 37 Galactic Cepheids were observed with the Spitzer Space Telescope; their mean magnitudes are provided in the MIR [3.6 μm] and [4.5 μm] filters by Monson et al. (2012). Similarly, 85 LMC Cepheid and 90 SMC Cepheid mean magnitudes were measured in the same filters by Scowcroft et al. (2011) and Scowcroft et al. (2016), respectively. These are internally photometrically consistent.

HST Wide Field Camera 3 (WFC3) filters. The HST WFC3 filters F555W, F814W, and F160W are particularly interesting, since they can be combined into the reddening-free Wesenheit index W_H, which is also used to observe extragalactic Cepheids (Riess et al. 2022), canceling photometric zero-point errors on the distance scale. Riess et al. (2021) provided HST/WFC3 photometry for 75 MW Cepheids obtained by the spatial scanning technique. Similarly, Riess et al. (2019) measured HST/WFC3 mean magnitudes in the same filters for 70 LMC Cepheids. Unfortunately, there is currently no available HST photometry for SMC Cepheids; in the HST photometric system, the analysis will be limited to Galactic and LMC Cepheids only.

Systematic uncertainties. In V, I, J, H, and K, the photometry for Galactic and Magellanic Cloud Cepheids was obtained with different instruments and sometimes in different systems (see Table 2); we include an error of 0.020 mag to the PL intercepts in these five filters for each host. For Gaia, Spitzer, and HST photometry, the data are taken with the same instruments and reduced by the same teams for the three galaxies so they do not require any systematic zero-point uncertainty.

Additionally, the Berdnikov (2008) catalog gathers observations made between 1986 and 2004 that are rather inhomogeneous; therefore, we quadratically include an additional photometric zero-point uncertainty of 0.010 mag for MW Cepheids in V and I, which sums to a total systematic zero-point difference between Cepheids in the MW and either Cloud of $\sigma = 0.03$ mag in these bands. For the LMC sample, M15 reported zero-point differences of 0.018 ± 0.067, -0.016 ± 0.058, and 0.000 ± 0.054 mag in J, H, and K, respectively, between M15 and Persson et al. (2004) after transformation into the 2MASS system. We adopt these values as photometric zero-point errors in the NIR for LMC Cepheids to account for the internal consistency of the M15 catalog. Finally, from the comparison between Kato et al. (2007) and VMC magnitudes in the SMC, a photometric zero-point uncertainty of 0.010 mag is adopted in the J, H, and K bands for the Cepheids of this galaxy.

2.2. Reddening

Apparent magnitudes must be carefully corrected for extinction, due to the presence of dust on the line of sight, using a reddening law and consistent $E(B-V)$ values. Past studies have relied on the Fernie et al. (1995) database, which is an inhomogeneous compilation of major color excess determinations published since 1975 derived from 17 sources of mostly photoelectric data in nonstandard bandpass systems that are therefore inadequate for providing consistent reddening estimates with an accuracy of a few hundredths of a magnitude across the sky needed for this study.

We make use of three different sources of reddening values for MW Cepheids. The first one is the 3D dust maps by Green et al. (2019) based on homogeneous Gaia, Pan-STARRS1, and 2MASS photometry. As a second method, we derive reddening values by comparing the observed color $(V-I)_{\rm obs}$ of Cepheids with their intrinsic color $(V-I)_{\rm intr}$ obtained from the period–color relation: $(V-I)_{\rm intr} = (0.25 \pm 0.01)\log P + (0.50 \pm 0.01)$ (Riess et al. 2022). Finally, we adopt as a third estimate the reddening values from Trahin et al. (2021) obtained with the SPIPS algorithm (Mérand et al. 2015) for MW Cepheids having an optimal set of spectro-, photo-, and interferometric data. In the Monte Carlo sampling procedure described in Section 3.3, $E(B-V)$ values are selected randomly among these three catalogs for each star, and the procedure is repeated over 10,000 iterations, which allows us to account for the covariance of these methods. Finally, in the LMC and SMC, we used the reddening maps by Skowron et al. (2021), and we transform $E(V-I)$ into $E(B-V)$ using the relation adopted by Skowron et al. (2021): $E(V-I) = 1.237 \times E(B-V)$. The MW Cepheids are particularly affected by interstellar reddening; the stars of our MW sample have a mean $E(B-V)$ of 0.5 mag (dispersion, $\sigma = 0.3$ mag), while in the LMC, they have a mean $E(B-V)$ of 0.11 mag ($\sigma = 0.05$ mag) and 0.05 mag ($\sigma = 0.02$ mag) in the SMC. Reddening uncertainties are propagated through uncertainty in the reddening law in the next section.

Table 3
Filters in Which the Effect of Metallicity Is Calibrated in This Study Effective central wavelength ($\lambda_0^{\rm eff}$) from the SVO filter profile service, ratios of total to selective absorption (R_λ) from Fitzpatrick (1999) assuming $R_V = 3.1 \pm 0.1$ (and from Indebetouw et al. 2005 for Spitzer bands), width of the instability strip (WIS), and mean metallicity of the MW sample

Filter	$\lambda_0^{\rm eff}$ (μm)	R_λ	WIS (mag)	$[{\rm Fe/H}]_{\rm MW}$ (dex)
BP	0.5036	3.433 ± 0.111	0.23	0.087 ± 0.056
V	0.5468	3.057 ± 0.099	0.22	0.093 ± 0.058
G	0.5822	2.783 ± 0.090	0.19	0.087 ± 0.056
RP	0.7620	1.831 ± 0.059	0.16	0.087 ± 0.056
I_C	0.7829	1.777 ± 0.057	0.14	0.097 ± 0.064
J	1.2350	0.812 ± 0.026	0.11	0.094 ± 0.081
H	1.6620	0.508 ± 0.016	0.09	0.094 ± 0.082
K	2.1590	0.349 ± 0.011	0.07	0.093 ± 0.087
[3.6 μm]	3.5075	0.198 ± 0.023	0.07	0.146 ± 0.075
[4.5 μm]	4.4366	0.152 ± 0.028	0.07	0.146 ± 0.075
		Wesenheit Indices		
W_G	$G - 1.900\,({\rm BP}-{\rm RP})$		0.10	0.087 ± 0.056
W_{VI}	$I - 1.387(V-I)$		0.077	0.098 ± 0.065
W_{JK}	$K - 0.735(J-K)$		0.086	0.094 ± 0.088
W_{VK}	$K - 0.127(V-K)$		0.077	0.098 ± 0.090
W_H	F160W − 0.386 (F555W − F814W)		0.069	0.099 ± 0.089

2.3. Metallicity

For MW Cepheids, we adopted in priority the iron abundances by Genovali et al. (2015) and complemented these values with the catalog by Genovali et al. (2014). The latter also provides additional abundances from the literature for 375 other Galactic Cepheids for which we set the uncertainty to 0.1 dex. All metallicity measurements provided in these catalogs are rescaled to the same solar abundance. The average metallicity of our full MW sample is +0.088 dex with a dispersion of 0.122 dex. However, the mean metallicity of MW Cepheids can differ depending on the sample (e.g., Cepheids for which we have optical photometry versus those for which we have NIR photometry); therefore, we consider the mean metallicity of the exact sample used in each filter. These mean values are similar in all filters (from +0.087 to +0.099 dex), except in the two Spitzer bands, where the mean metallicity is slightly higher (+0.146 dex), which can be explained by the small size of the sample. In order to derive the uncertainties for the mean MW metallicity in each filter, we run a bootstrap algorithm on the available metallicity values and adopt the 99% confidence interval (3σ) of the distribution of the mean values. Considering the limited size of our metallicity sample, particularly in the Spitzer bands, the bootstrapping approach enables us to determine the confidence interval of the mean metallicity without an assumption of the normality of the metallicity sample distribution (Efron & Tibshirani 1986). These values are listed in Table 3.

We note that additional constraining power is available by retaining the individual MW abundances in the analysis (Riess et al. 2021), but we have chosen the simpler host-to-host analysis for its transparency, although it relies on the use of a single average MW metallicity.

Romaniello et al. (2022) recently obtained high-resolution spectra for 89 Cepheids in the LMC, derived their chemical abundances, and revised the measurements of those from Romaniello et al. (2008). They concluded that they are

consistent within the errors with a single common abundance of −0.409 dex with a dispersion of 0.076 dex (similar to the uncertainty per measurement of 0.07 dex), which is more metal-poor by 0.1 dex, and the breadth of the distribution is half as wide (see discussion in Romaniello et al. 2022). We adopt this mean value for all LMC Cepheids with an uncertainty of 0.02 dex. In the SMC, we follow Gieren et al. (2018) and adopt a mean metal abundance of -0.75 ± 0.05 dex for all SMC Cepheids (see discussion in Section 5.4).

2.4. Distances

Distances to MW Cepheids are taken from the Bailer-Jones et al. (2021) catalog based on the Gaia EDR3 parallaxes (Gaia Collaboration et al. 2022), as well as the associated uncertainties; we adopted the photogeometric distances that are derived using the (BP − RP) color, G magnitude, Gaia EDR3 parallaxes, and a direction-dependent prior accounting for the distribution of stellar distances along a line of sight and interstellar extinction. These distances include the Lindegren et al. (2021) zero-point correction on Gaia parallaxes. Lindegren et al. (2021) recommended including an error of a few μas on the parallax zero-point, so we assumed a 5 μas uncertainty, which is equivalent to including a systematic error of ∼0.02 mag in terms of distance modulus for this sample of MW Cepheids.

The MW Cepheids are much brighter than most stars in the Gaia catalog with visual magnitudes of 6–9 mag, brighter than the range where the Gaia zero-point is well calibrated. As a result, it is recommended by the Gaia team to derive the zero-point in this magnitude range independently from the luminosity using the PL relation. Following this procedure, Riess et al. (2021) found that the Lindegren et al. (2021) zero-point is overestimated by approximately 14 μas, which was confirmed by Zinn (2021) from asteroseismology of bright red giants independently of the PL relation. We therefore applied a small additional correction (dr) to the Bailer-Jones et al. (2021) distances in order to take this zero-point into account. A good approximation[6] of this correction is to take $dr = -r^2\, d\varpi$, where $d\varpi = -0.014$ mas, and r is the original Bailer-Jones et al. (2021) distance in kiloparsecs. Finally, all Cepheids with a renormalized unit weight error (RUWE) parameter larger than 1.4 were excluded from the sample as likely astrometric binaries.

For LMC Cepheids, we adopt the most precise distance to this galaxy obtained by Pietrzyński et al. (2019) from a sample of 20 DEBs: 49.59 ± 0.09 (stat.) ± 0.54 (syst.) kpc. This corresponds to a full uncertainty of 0.026 mag in distance modulus. For more precision on the adopted distance, the position of each Cepheid in the LMC is taken into account by applying the planar geometry correction by Jacyszyn-Dobrzeniecka et al. (2016; see B21).

[6] The best way to include the additional 0.014 mas offset would be to infer new corrected distances for all of our MW Cepheids using the Bailer-Jones et al. (2021) method; however, it would be beyond the scope of this paper and would give similar results in terms of precision. In particular, running the Bailer-Jones method for such a large number of stars is very time consuming (CPU); therefore, it was tested for a few stars only (C. Bailer-Jones 2022, private communication; we do not have access to the code to produce these distances). We selected a few Cepheids with low (1%), typical (3%), and high (10%) parallax uncertainties for which the Bailer-Jones distances were recomputed after including the additional 0.014 mas offset. The approximated correction reproduces these values to 0.1% or better, regardless of the parallax precision.

With the same technique and assumptions, Graczyk et al. (2020) published the most precise distance to the SMC from 15 eclipsing binary systems distributed around the core; they obtained a distance of 62.44 ± 0.47 (stat.) ± 0.81 (syst.) kpc. This is equivalent to a full uncertainty of 0.032 mag in distance modulus. To account for the elongated shape of the SMC along the line of sight, we include the geometric model fit to the DEBs and described by the blue lines in Figure 4 of Graczyk et al. (2020); their equations are provided in B21 (we also limit the selection of SMC Cepheids to a separation of $<0\overset{\circ}{.}6$ between the Cepheids and the SMC center, which, together with the geometric correction we show greatly reduces their dispersion; see Sections 3.1 and 5.5). Following Riess et al. (2019), we include these corrections directly on Cepheid magnitudes. Considering the standard deviation of three different geometry models, Riess et al. (2019) found a systematic uncertainty of 0.002 mag associated with the LMC geometry; we neglected this contribution to the error budget, since it is widely dominated by other systematics.

3. Method

3.1. Sample Selection

Among the Cepheid samples described in the previous section, a selection based on various criteria is performed. First, only fundamental-mode Cepheids are considered; in the MW, the pulsation modes are taken from the new Gaia DR3 reclassification by Ripepi et al. (2022c; see their Table 6). First-overtone and mixed-mode pulsators were discarded. A second selection is performed based on the number of epochs available for a given light curve. For the MW sample, only Cepheids with at least eight data points are considered. Regarding the LMC and SMC samples, a large number of Cepheids have less than eight measurements per light curve in the NIR, and excluding them would drastically reduce the sample; therefore, a limit of five epochs per star is adopted. For all Cepheids, a minimum uncertainty of 10% on mean magnitudes is adopted as a precision limit. Additionally, due to the nonnegligible depth of the Magellanic Clouds (especially that of the SMC), Cepheids outside of a radius of 3° around the LMC center and $0\overset{\circ}{.}6$ around the SMC center are excluded from the analysis. These regions are found to be optimal, as they minimize the scatter of the PL relation (see Section 5.5) and, together with the geometric correction, reduce any potential separation from the mean of the DEBs.

Finally, a break in the PL/period-Wesenheit relations was identified in the SMC in both the optical and the NIR; the position of this break was found around $\log P \sim 0.4$ by Udalski et al. (1999), Sharpee et al. (2002), Sandage et al. (2009), and Soszyński et al. (2010). Tammann et al. (2011) reported a break at a larger period around $\log P \sim 0.55$, and more recently, Subramanian & Subramaniam (2015) and Ripepi et al. (2016) detected a break at $\log P \sim 0.47$. We perform a cut at $\log P = 0.47$ in the SMC due to this nonlinearity but also at $\log P = 0.4$ in the MW and LMC and $\log P = 2$ in the three galaxies, which allows the prevention of undesirable effects such as confusion of pulsation modes and possible (although not yet detected) breaks at shorter or longer periods. Since the MW and LMC were found to be linear (Inno et al. 2016; Ripepi et al. 2022b), the period cut does not affect the slope of these samples. For example, changing the break period from

$\log P \sim 0.4$ to 0.47 only changes the LMC slope by a few mmag dex^{-1} and does not impact the results of our analysis.

3.2. Width of the Instability Strip

The finite width of the instability introduces additional scatter in the PL relation and should be included quadratically as an uncertainty in apparent magnitudes. In Riess et al. (2019), the width of the instability strip is obtained by taking the scatter of the PL relation (0.075 mag from their Table 3) and quadratically subtracting the errors on photometric measurements (e.g., photometric inhomogeneities, phase corrections), which are of 0.030 mag. They obtained an intrinsic width of 0.069 mag for the instability strip in the W_H index. Similarly, the values in the V and I bands are 0.22 and 0.14 mag (Macri et al. 2006). In the J, H, and K bands, the study by Persson et al. (2004) gives a width of 0.11, 0.09, and 0.07 mag for the NIR instability strip. For the Spitzer bands, we adopt a width of 0.07 mag (Scowcroft et al. 2011; Monson et al. 2012). In the Gaia bands G, BP, and RP, as well as the Gaia Wesenheit W_G, we adopt for the width of the instability strip the PL dispersion obtained in the LMC by Ripepi et al. (2019; see their Table 1): 0.19, 0.23, 0.16, and 0.10 mag, respectively. Although their magnitudes are not dereddened, the reddening in the LMC is limited and homogeneous, and the small fraction of highly reddened Cepheids has little impact on the scatter of the PL relation. Indeed, according to Ripepi et al. (2019), the scatter decreases from BP to G and from G to RP, as expected, and is perfectly consistent with the width adopted for the other filters. For the W_{VI} Wesenheit magnitudes, we adopt a width of 0.077 mag from Soszyński et al. (2015). Finally, in W_{JK} and W_{VK}, we adopt a width of 0.086 and 0.077 mag, respectively, from the study by Ripepi et al. (2022a) that gives a scatter of 0.088 and 0.080 mag, respectively, and photometric errors of the order of 0.020 mag.

3.3. Period–Luminosity–Metallicity Relation

The absolute magnitude M_λ of a star is derived from its apparent magnitude m_λ, reddening $E(B-V)$, and distance d in kiloparsecs by the equation

$$M_\lambda = m_\lambda - R_\lambda E(B-V) - 5\log d - 10. \quad (2)$$

Apparent magnitudes are corrected for extinction using the standard reddening law from Fitzpatrick (1999) for our G, BP, RP, V, I, J, H, and K_S magnitudes and the reddening law from Indebetouw et al. (2005) for Spitzer filters. We set the R_V parameter to 3.1 ± 0.1, which yields the R_λ values listed in Table 3. The uncertainty of 0.1 in R_V and its propagation to other filters is intended to characterize the line-of-sight dispersion seen for similar stellar populations (see discussion in Section 5.3). Five Wesenheit indices are also considered (Madore 1982) based on a combination of optical and NIR filters, such that $W(\lambda_1, \lambda_2, \lambda_3) = m_{\lambda_1} - R\,(m_{\lambda_2} - m_{\lambda_3})$ with $R = R_{\lambda_1}/(R_{\lambda_2} - R_{\lambda_3})$. For the HST Wesenheit W_H, we adopt $R = 0.386$ from Riess et al. (2022), and for the Gaia Wesenheit index W_G, we use $R = 1.90$ for consistency with Ripepi et al. (2022c).

To measure the metallicity effect γ between the Galactic, LMC and SMC samples, the PL relation of the form

$$M = \alpha\,(\log P - \log P_0) + \beta \quad (3)$$

is first fitted in each of the three galaxies, with a common slope α fixed to that of the LMC (since it has the largest number of Cepheids, the lowest PL dispersion, and the slope least affected by nonuniformity of individual Cepheid distances). The three PL intercepts β are obtained from Monte Carlo sampling of the data and error distributions with 10,000 iterations; to ensure the robustness of the fit, the apparent magnitudes, distances, R_V, and $E(B-V)$ values are free to vary within the uncertainties during each iteration. In the case of the MW sample, the $E(B-V)$ values are selected randomly for each star among the three previously described measures of extinction (see Table 2), which will naturally account for their covariance. Systematic uncertainties due to photometric zero-points (see Section 2.1) and distance measurements (see Section 2.4) are included quadratically to the intercept errors in the three galaxies. Finally, the metallicity term γ of the PL relation as defined in Equation (1) is obtained by fitting (again with Monte Carlo sampling) the relation

$$\beta = \gamma\,[\mathrm{Fe/H}] + \delta, \quad (4)$$

where β is the PL intercept, [Fe/H] is the mean metallicity in each of the three galaxies, and δ is the fiducial luminosity at $\log P = 0.7$ and solar metallicity. As an example, Figure 1 illustrates the linear fit of Equation (4) in the W_{JK} band.

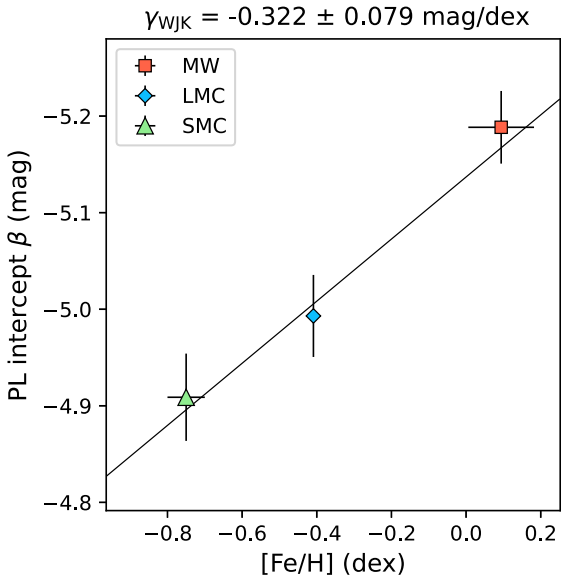

Figure 1. The PL intercept (β) in the W_{JK} Wesenheit index fitted with a common slope in the MW, LMC, and SMC as a function of the mean metallicity ([Fe/H]) of the galaxy (Equation (4)).

4. Results

4.1. The PL Relation

In Section 4.2, the metallicity term (γ) of the PL relation will be derived when the slopes (α) are fixed to the same value in the three galaxies in order to directly compare the intercepts (β). However, in this section, we first calibrate the PL relation of the form $M = \alpha(\log P - 0.7) + \beta$ in each galaxy, where both the slope and the intercept are free to vary. This allows one to check the consistency of the slopes in the three galaxies. The coefficients are listed in Table 4 and represented in Figure 2.

Generally, the PL slope obtained for the LMC sample agrees to better than 3σ with that of the MW and SMC samples. The

Table 4
Results of the PL Fit of the Form $M = \alpha(\log P - 0.7) + \beta$ in the MW, LMC, and SMC

Filter	Galaxy	$\alpha_{\rm free}$	$\beta_{\rm free}$	$\alpha_{\rm fixed}$	β	σ	$N_{\rm stars}$
	MW	-2.888 ± 0.069	-3.197 ± 0.069	-2.634 ± 0.030	-3.236 ± 0.075	0.56	445
BP	LMC	-2.634 ± 0.030	-3.063 ± 0.013	-2.634 ± 0.030	-3.063 ± 0.029	0.23	1593
	SMC	-2.523 ± 0.070	-2.961 ± 0.018	-2.634 ± 0.030	-2.957 ± 0.037	0.29	287
	MW	-2.631 ± 0.087	-3.356 ± 0.049	-2.715 ± 0.029	-3.338 ± 0.060	0.22	183
V	LMC	-2.715 ± 0.029	-3.191 ± 0.011	-2.715 ± 0.029	-3.191 ± 0.035	0.21	1609
	SMC	-2.596 ± 0.067	-3.079 ± 0.018	-2.715 ± 0.029	-3.074 ± 0.041	0.28	291
	MW	-3.112 ± 0.060	-3.578 ± 0.058	-2.816 ± 0.025	-3.623 ± 0.064	0.49	446
G	LMC	-2.816 ± 0.025	-3.335 ± 0.010	-2.816 ± 0.025	-3.335 ± 0.028	0.18	1602
	SMC	-2.758 ± 0.059	-3.221 ± 0.016	-2.816 ± 0.025	-3.218 ± 0.036	0.25	288
	MW	-3.037 ± 0.046	-3.850 ± 0.042	-2.918 ± 0.019	-3.868 ± 0.047	0.44	446
RP	LMC	-2.918 ± 0.019	-3.812 ± 0.008	-2.918 ± 0.019	-3.813 ± 0.027	0.16	1584
	SMC	-2.853 ± 0.044	-3.722 ± 0.012	-2.918 ± 0.019	-3.718 ± 0.034	0.22	287
	MW	-2.858 ± 0.063	-4.005 ± 0.031	-2.950 ± 0.018	-3.988 ± 0.043	0.19	157
I	LMC	-2.950 ± 0.018	-3.851 ± 0.007	-2.950 ± 0.018	-3.851 ± 0.034	0.14	1687
	SMC	-2.971 ± 0.040	-3.772 ± 0.010	-2.950 ± 0.018	-3.770 ± 0.039	0.21	300
	MW	-3.207 ± 0.075	-4.525 ± 0.028	-3.097 ± 0.013	-4.548 ± 0.036	0.19	71
J	LMC	-3.097 ± 0.013	-4.335 ± 0.004	-3.097 ± 0.013	-4.335 ± 0.038	0.13	1644
	SMC	-3.001 ± 0.026	-4.292 ± 0.007	-3.097 ± 0.013	-4.287 ± 0.040	0.17	299
	MW	-3.296 ± 0.066	-4.787 ± 0.022	-3.161 ± 0.013	-4.816 ± 0.033	0.18	70
H	LMC	-3.161 ± 0.013	-4.677 ± 0.004	-3.161 ± 0.013	-4.677 ± 0.037	0.09	751
	SMC	-3.207 ± 0.023	-4.578 ± 0.006	-3.161 ± 0.013	-4.581 ± 0.039	0.17	290
	MW	-3.235 ± 0.065	-4.929 ± 0.021	-3.222 ± 0.008	-4.932 ± 0.033	0.17	65
K	LMC	-3.222 ± 0.008	-4.713 ± 0.002	-3.222 ± 0.008	-4.713 ± 0.033	0.09	1653
	SMC	-3.198 ± 0.017	-4.649 ± 0.004	-3.223 ± 0.008	-4.647 ± 0.039	0.15	299
	MW	-3.457 ± 0.076	-4.922 ± 0.037	-3.324 ± 0.038	-4.968 ± 0.032	0.20	21
[3.6 μm]	LMC	-3.324 ± 0.038	-4.791 ± 0.024	-3.324 ± 0.038	-4.791 ± 0.027	0.11	66
	SMC	-3.615 ± 0.063	-4.539 ± 0.038	-3.324 ± 0.038	-4.703 ± 0.036	0.12	23
	MW	-3.365 ± 0.074	-4.913 ± 0.037	-3.233 ± 0.040	-4.961 ± 0.034	0.21	21
[4.5 μm]	LMC	-3.233 ± 0.040	-4.821 ± 0.024	-3.233 ± 0.040	-4.821 ± 0.027	0.11	66
	SMC	-3.582 ± 0.064	-4.574 ± 0.037	-3.233 ± 0.040	-4.770 ± 0.035	0.14	23
	MW	-3.422 ± 0.026	-4.995 ± 0.007	-3.338 ± 0.012	-5.005 ± 0.021	0.32	596
W_G	LMC	-3.338 ± 0.012	-4.791 ± 0.003	-3.338 ± 0.012	-4.791 ± 0.026	0.11	1591
	SMC	-3.388 ± 0.025	-4.683 ± 0.006	-3.338 ± 0.012	-4.686 ± 0.033	0.14	286
	MW	-3.197 ± 0.036	-4.913 ± 0.011	-3.291 ± 0.010	-4.895 ± 0.038	0.18	157
W_{VI}	LMC	-3.291 ± 0.010	-4.771 ± 0.002	-3.291 ± 0.010	-4.771 ± 0.038	0.09	1606
	SMC	-3.317 ± 0.021	-4.726 ± 0.005	-3.291 ± 0.010	-4.728 ± 0.043	0.13	288
	MW	-3.345 ± 0.064	-5.182 ± 0.022	-3.323 ± 0.009	-5.188 ± 0.038	0.18	63
W_{JK}	LMC	-3.323 ± 0.009	-4.993 ± 0.002	-3.323 ± 0.009	-4.993 ± 0.042	0.09	1653
	SMC	-3.350 ± 0.018	-4.907 ± 0.005	-3.323 ± 0.009	-4.909 ± 0.045	0.13	298
	MW	-3.246 ± 0.068	-5.149 ± 0.021	-3.255 ± 0.011	-5.146 ± 0.039	0.21	57
W_{VK}	LMC	-3.255 ± 0.011	-4.905 ± 0.002	-3.255 ± 0.011	-4.905 ± 0.038	0.08	1500
	SMC	-3.293 ± 0.018	-4.844 ± 0.005	-3.255 ± 0.011	-4.847 ± 0.044	0.14	288
	MW	-3.361 ± 0.056	-4.949 ± 0.019	-3.305 ± 0.038	-4.964 ± 0.024	0.16	60
W_H	LMC	-3.305 ± 0.038	-4.816 ± 0.018	-3.305 ± 0.038	-4.823 ± 0.027	0.08	70
	SMC	...	...	...	...	...	...

Note. In the third and fourth columns, $\alpha_{\rm free}$ and $\beta_{\rm free}$ are obtained when both coefficients are free parameters. In the fifth and sixth columns, β is the intercept obtained with the slope $\alpha_{\rm fixed}$ fixed to that of the LMC.

only exceptions are the G and BP bands, where the MW and LMC slopes differ by 4σ and 3σ, respectively; both Spitzer bands, where the LMC slope is shallower than in the SMC by 4σ; and the J filter, where the LMC and SMC PL slopes differ by 3.3σ. However, we see no strong evidence to reject the hypothesis of a common slope in the three galaxies (see Section 4.2); the disagreement between the LMC and SMC slopes in both Spitzer filters can be traced back to the strict selection of the core region of the SMC ($R < 0.^{\circ}6$), which only leaves 22 out of the 90 original Cepheids. When including all 90 Cepheids from the SMC sample, we can closely reproduce the slopes reported by Scowcroft et al. (2016). In Section 5.2,

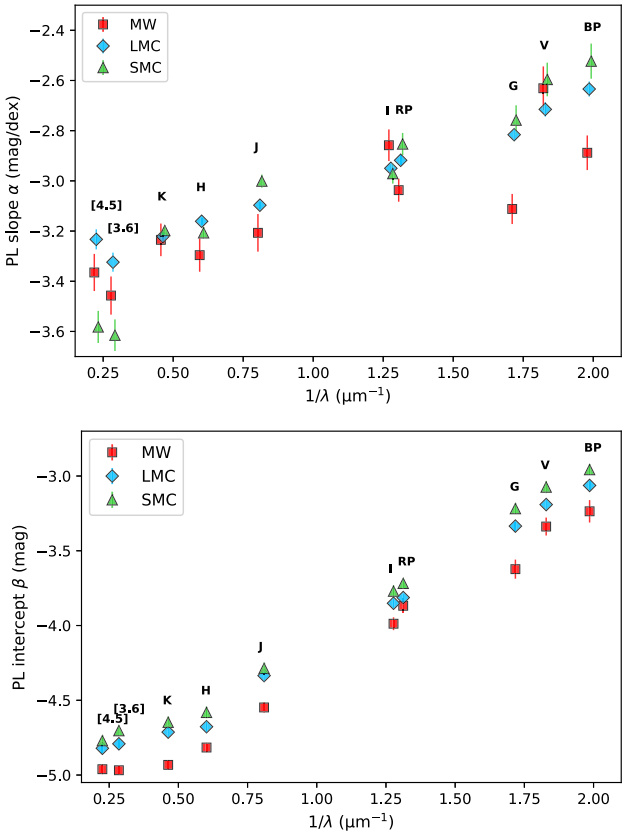

Figure 2. Top: PL slope (α) in the MW and Magellanic Clouds represented with the inverse of wavelength. Bottom: PL intercept (β) obtained in the MW and Magellanic Clouds with a slope fixed to that of the LMC, represented with the inverse of wavelength.

we discuss the impact of the SMC sample selection on the values of γ. In J, adopting the SMC slope instead of the LMC slope changes the γ parameter by only 0.014 mag dex^{-1}, which is negligible compared to the uncertainties. Finally, adopting the MW slope in the Gaia filters changes the γ term by 0.013 mag at most.

We also note that our PL slopes in the three galaxies are in excellent agreement with those reported by Ripepi et al. (2022c) in the G and W_G filters. Our slopes agree well with Subramanian & Subramaniam (2015) in V and I and Ripepi et al. (2016) in J, K, W_{JK}, and W_{VK} for the SMC sample.

As expected, the dispersion of the PL relation decreases from the optical to the infrared, which is a consequence of the sensitivity of each filter to the extinction and the width of the instability strip. In the MW, as well as in both Magellanic Clouds, the PL slope α generally becomes steeper, and the PL intercept β becomes more negative (i.e., brighter) from the optical toward the infrared. Due to the presence of a large CO absorption band aligned with the [4.5 μm] filter (Marengo et al. 2010; Freedman et al. 2011; Scowcroft et al. 2011), in Section 5.2, the [4.5 μm] filter is ignored in the fit of the $\gamma = f(\lambda)$ relation. In the Wesenheit W_H band, we obtain a slope of -3.305 ± 0.038 mag dex^{-1} in the LMC, which is fully compatible with the slope of -3.299 ± 0.015 mag dex^{-1} derived by the SH0ES team (Riess et al. 2022).

In the MW, the PL relation generally shows a larger dispersion than in the Magellanic Clouds because of the higher extinction and nonuniform distances. The PL relations in the Wesenheit indices show a low dispersion, as expected from their insensitivity to extinction. In some filters, only a small number of Cepheids is listed in Table 4; this is due to the various selection criteria applied to the samples, such as the upper limit of 1.4 on the RUWE parameter, the limited radius around the SMC center, and the cuts in periods. Finally, for a given filter, the PL intercept in the MW is more negative than in the LMC and even more than in the SMC (see Figure 2), indicating a negative sign for the γ term.

Table 5
Results of the Fit of the Form $\beta = \gamma$ [Fe/H] + δ (Equation (4)) Obtained from a Comparison of the PL Intercepts (β) in the MW, LMC, and SMC

Filter	γ	σ	δ	σ	$N_{\rm stars}$
BP	−0.320	0.095	−3.194	0.050	2325
V	−0.311	0.082	−3.314	0.046	2083
G	−0.462	0.089	−3.539	0.047	2336
RP	−0.178	0.068	−3.873	0.036	2317
I	−0.247	0.068	−3.956	0.038	2144
J	−0.294	0.066	−4.478	0.037	2014
H	−0.275	0.065	−4.789	0.036	1111
K	−0.321	0.068	−4.860	0.034	2017
[3.6 μm]	−0.292	0.057	−4.915	0.031	110
[4.5 μm]	−0.204	0.057	−4.911	0.029	110
W_G	−0.384	0.051	−4.958	0.025	2473
W_{VI}	−0.201	0.071	−4.864	0.035	2051
W_{JK}	−0.322	0.079	−5.137	0.042	2014
W_{VK}	−0.332	0.081	−5.066	0.042	1845
W_H[a]	−0.280	0.078	−4.939	0.027	130

Note. The slope α is fixed to that of the LMC sample (see Table 4).
[a] Does not include the SMC sample (no HST photometry) or individual metallicities in the MW or Cepheids in SN Ia hosts as used in Riess et al. (2022).

4.2. The PLZ Relation

After fixing the PL slope to that of the LMC (Table 4) in the three galaxies, we solve for Equation (4) with a Monte Carlo sampling, where both the intercepts (β) and the mean [Fe/H] values of each sample are free to vary within their error bars. The γ and δ coefficients obtained for the PLZ relation are listed in Table 5.

All γ values over a wavelength range of 0.5–4.5 μm are negative (with a significance of 2.6σ–7.5σ), meaning that metal-rich Cepheids are brighter than metal-poor ones. The γ values range between a minimum of -0.178 ± 0.068 mag dex^{-1} (in RP) and a maximum of -0.462 ± 0.089 mag dex^{-1} (in G) with a dispersion of 0.05 mag dex^{-1}. In all filters, the γ values are in good agreement with those obtained by Gieren et al. (2018) and B21, especially in the NIR, but significantly stronger than the effect detected by Wielgórski et al. (2017), which was close to zero (see discussion in Section 5.5). The metallicity effect in the Gaia filters is similar to that in ground optical filters (V, I); however the G band and W_G Wesenheit index show a stronger effect (see discussion in Section 5.1).

We tested the hypothesis of a common slope in the three galaxies by fixing the slope to that of the SMC instead of that of the LMC; we obtained similar γ values at the 0.8σ level or better, confirming the validity of our hypothesis.

5. Discussion

5.1. Potential Issues with the Gaia Wesenheit Index

In the Gaia Wesenheit index W_G, we derive a strong effect of -0.384 ± 0.051 mag dex^{-1}, slightly shallower but still close to

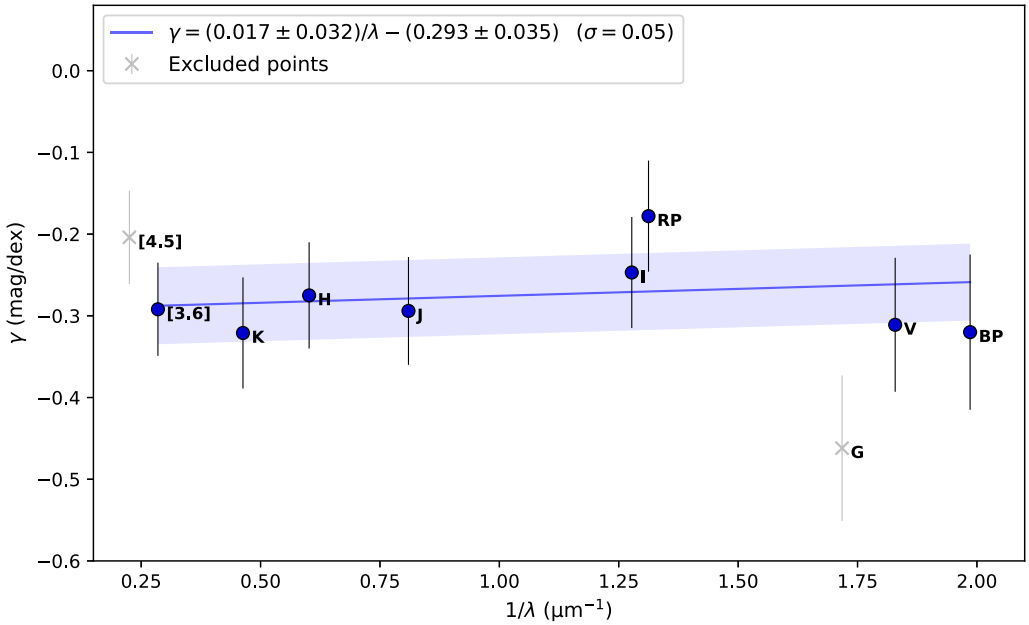

Figure 3. Metallicity effect (γ) as a function of the inverse of wavelength ($1/\lambda$).

the previous result by Ripepi et al. (2022a), who obtained -0.520 ± 0.090 mag dex^{-1} from MW Cepheids. The metallicity effect in this Wesenheit index is surprisingly strong compared to other filters or Wesenheit indices but comparable to that in the Gaia G band (-0.462 ± 0.089 mag dex^{-1}). This could be explained by the particularly large width of the G filter (almost 800 nm) and suggests that the results based on Gaia G-band photometry should be treated particularly carefully. For these reasons, the G band is ignored in the fit of the relation between γ and λ in Figure 3. Additionally, Wesenheit indices have been established to minimize the effects of interstellar extinction; however, they are not totally independent of the reddening law, since they rely on the R coefficient (see Section 3).

5.2. A Relationship between γ and λ

As the filters used in this analysis cover a large wavelength range, we can measure a dependence between the metallicity term γ and the wavelength. When fitting a linear relationship between γ and $1/\lambda$ through the points of Figure 3 after excluding the [4.5 μm] filter (see Section 4.1) and the G band (see Section 5.1), we derive the following relation:

$$\gamma = \frac{0.017 \pm 0.032}{\lambda} - (0.293 \pm 0.035) \text{ mag dex}^{-1}, \quad (5)$$

with $\sigma = 0.05$ mag dex^{-1}. The slope of Equation (5) shows that the metallicity effect is mostly uniform over the wavelength range 0.5–4.5 μm. Compared to the luminosity dependence, it indicates that Cepheid colors are relatively insensitive to metallicity.

To verify that this is not related to any use of Cepheid colors in reddening measurements, we repeated the analysis after discarding reddening estimates based on color (i.e., only the reddening maps by Green et al. 2019 are used); we obtain a similar dependence ($\gamma \sim 0.038 \pm 0.043/\lambda$), which confirms the previous finding.

As mentioned in Section 4.1, the PL slope in the Spitzer bands for the SMC sample depends on the adopted region around the SMC center. The selection corresponding to $R < 0.^{\circ}6$ excludes a large fraction of the initial sample and returns PL slopes that are more negative than expected. With a more moderate selection of $R < 1.^{\circ}2$, the SMC slopes are in better agreement with Scowcroft et al. (2016), and the γ values become slightly shallower, with -0.279 ± 0.060 and -0.194 ± 0.056 mag dex^{-1} in [3.6 μm] and [4.5 μm], respectively. This would revise Equation (5) to $\gamma = (0.012 \pm 0.032)/\lambda - (0.286 \pm 0.035)$ mag dex^{-1}.

5.3. Reddening Law

The correction for dust extinction and the assumption of a reddening law are critical steps in the calibration of the distance scale. The parameter $R_V = A_V/E(B-V)$ is related to the average size of the dust grains and gives a physical basis for the variations in extinction curves. Although the differences in R_V are relatively small between the MW and Magellanic Clouds, they can still impact the calibration of the Leavitt law. In the MW, most studies are based on the assumption $R_V = 3.1$ (Cardelli et al. 1989), while Gordon et al. (2003) reported an average of $R_V = 3.41 \pm 0.06$ in the LMC and $R_V = 2.74 \pm 0.13$ in the SMC. They concluded that LMC and SMC extinction curves are qualitatively similar to those derived in the MW. But even in the MW, the extinction curve was shown to be highly spatially variable (Fitzpatrick et al. 2019).

Assuming a different reddening law or R_V value across different galaxies is possible but more complex (see Riess et al. 2022, Appendix D); since the R ratio in the Wesenheit indices multiplies a color term, it requires separating the contribution of the color that results from dust reddening by first subtracting the intrinsic color of the Cepheids, which can be done using a period–color relation. However, Riess et al. (2022) concluded that determining individual values of R was not very informative due to large uncertainties on both color and brightness.

In the present work, we adopted the standard reddening law from Fitzpatrick (1999) for our G, BP, RP, V, I, J, H, and K_S magnitudes and the reddening law from Indebetouw et al. (2005) for Spitzer filters with a uniform R_V value of 3.1 ± 0.1.

We note that the uncertainty on this parameter is usually neglected in most studies, even when combining Cepheid samples in different galaxies (e.g., Wielgórski et al. 2017; Gieren et al. 2018; Owens et al. 2022). While it is a reasonable assumption for the MW and LMC, the SMC is likely to have a lower R_V value (Gordon et al. 2003); however, this value has not been measured for our population of Cepheids, so it is still unclear whether it applies to the present sample. For simplicity and consistency between the three galaxies, we assumed the same R_V in the three samples. For each filter, we also included the uncertainties on the A_λ/A_V ratios by varying R_V by ± 0.1 with the `dust_extinction` Python package.[7]

While it is not recommended to vary R_V between host galaxies for Wesenheit indices (Riess et al. 2022, Appendix D), we tested the effect of changing the R_V value to 2.74 ± 0.13 in the SMC for single filters only. We find that the metallicity effect becomes stronger in an absolute sense (i.e., more negative) by 0.020–0.040 mag dex^{-1} in the optical bands and at most 0.008 mag dex^{-1} in the NIR. These changes are well within the error bars listed in Table 5 and result in a shallower dependence between γ and wavelength, with Equation (5) becoming $\gamma = (0.005 \pm 0.035)/\lambda - (0.288 \pm 0.039)$ mag dex^{-2}.

5.4. SMC Mean Metallicity

In the Romaniello et al. (2022) reanalysis of the LMC metallicity, a shift of 0.07 dex was detected compared with the previous value by Romaniello et al. (2008). This offset is due to a difference in temperature in the abundance analysis. In light of this reanalysis, we can reasonably expect a similar shift in the SMC mean metallicity; following the same procedure, it is plausible that a reanalysis of the original SMC data leads to a revised value of about $[\mathrm{Fe/H}] = -0.90 \pm 0.05$ dex. While a more detailed analysis is required before adopting this value as our final SMC metallicity, we can easily measure the impact that this change would have on the γ values. Replacing the original SMC metallicity of -0.75 dex by a more metal-poor value of -0.90 dex gives shallower values of the metallicity effect. Typically, the gamma values change by 0.020 mag dex^{-1} (e.g., in RP) to 0.055 mag dex^{-1} (e.g., in *JHK*), which is comprised within the error bars. Overall, this change in the SMC metallicity results in a shallower dependence between γ and the effective wavelength, with $\gamma = (0.007 \pm 0.024)/\lambda - (0.235 \pm 0.026)$ mag dex^{-1} (see Figure 7 in the Appendix).

If the SMC metallicity was to be revised to a more metal-poor value, this would not affect the main conclusion of the present work (γ mostly independent of wavelength), and the updated γ values would still be in excellent agreement with other findings from the literature.

5.5. Comparison with Other Empirical Estimates of γ

The recognition of a γ term is relatively recent, owing to the necessary improvements in data quality (i.e., parallaxes, reddenings, Cepheid photometry, metallicity, and Cloud geometry) that have accrued in the last two decades. In this section, we aim at identifying sources of differences with some previous studies. We represent some of these previously published values of the metallicity effect in Figure 4.

[7] https://dust-extinction.readthedocs.io/en/stable/

In W_{VI}, our value of $\gamma = -0.201 \pm 0.071$ mag dex^{-1} agrees well with early estimates by Kennicutt & Stetson (1998), Sakai et al. (2004), Macri et al. (2006), and Scowcroft et al. (2009). In all filters, we find a stronger negative metallicity effect than Storm et al. (2011a) and Groenewegen (2013), who both used Baade–Wesselink distances and reported γ values mostly consistent with zero. Gieren et al. (2018) also adopted a similar approach but measured a stronger effect (around -0.27 mag dex^{-1}), consistent with the present study although with larger error bars. Groenewegen (2018) obtained a shallower metallicity effect in V, K, and W_{VK} based on Gaia DR2 parallaxes but still comparable with our findings within the error bars, similar to Ripepi et al. (2020). The results by Ripepi et al. (2021) based on Gaia EDR3 parallaxes are close to our values in K, W_{JK}, and W_{VK} in the sense that they show a strong effect, although their values are more negative by about 0.1 mag dex^{-1}. Recently, Cruz Reyes & Anderson (2022) compared a sample of MW open clusters with the LMC Leavitt law and obtained γ values in G, BP, RP, I, W_{VI}, W_G, and W_H that are in good agreement with our findings. Finally, in the W_H Wesenheit index based on pure HST photometry of MW and LMC Cepheids, we obtain a metallicity effect of -0.280 ± 0.078 mag dex^{-1}, in agreement with the value of -0.217 ± 0.046 mag dex^{-1} derived by the SH0ES team from a broader range of data from the MW, LMC, SMC, NGC 4258, and gradients in SN Ia hosts (Riess et al. 2022).

Freedman & Madore (2011) used spectroscopic [Fe/H] abundances of 22 individual LMC Cepheids whose metallicities were measured by Romaniello et al. (2008), covering a range of about 0.6 dex. They derived a negative metallicity effect in the MIR, canceling in the NIR and becoming positive in optical wavelengths. However, Romaniello et al. (2022) published new abundances for a larger sample of LMC Cepheids and this time reported a very narrow distribution of metallicities ($\sigma = 0.1$ dex including systematics). They also noted that the abundances provided in Romaniello et al. (2008) were significantly affected by a systematic error in the data reduction and analysis, and they confirmed that the previous data are compatible with the same narrow spread observed for the new values. This shows that the LMC cannot be used to internally measure the metallicity effect and explains the differences in the findings of Freedman & Madore (2011; see Romaniello et al. 2022, for further discussion).

Wielgórski et al. (2017) performed a purely differential calibration of the γ term by comparing the Leavitt law across the full span of the LMC and SMC. Assuming the DEB distance by Pietrzyński et al. (2013) and Graczyk et al. (2014), respectively, they obtained a metallicity effect consistent with zero in the optical and NIR. Updating the mean LMC metallicity with the recent value by Romaniello et al. (2022) and/or replacing the DEB distances with the most precise ones by Pietrzyński et al. (2019) and Graczyk et al. (2020) does not yield significant differences with the Wielgórski et al. (2017) results. However, we find that the size of the region and its depth considered around the SMC center considerably impact the value of the γ term. The sensitivity of γ to the size of the region adopted in the SMC is due to the elongated shape of this galaxy along the line of sight. Despite the geometry correction performed in Section 2.4, Cepheids at larger distances to the SMC center show a larger scatter, as shown in Figure 5, likely due to the shortcomings of the planar model at greater radii (and farther from the region, it was defined by the DEBs).

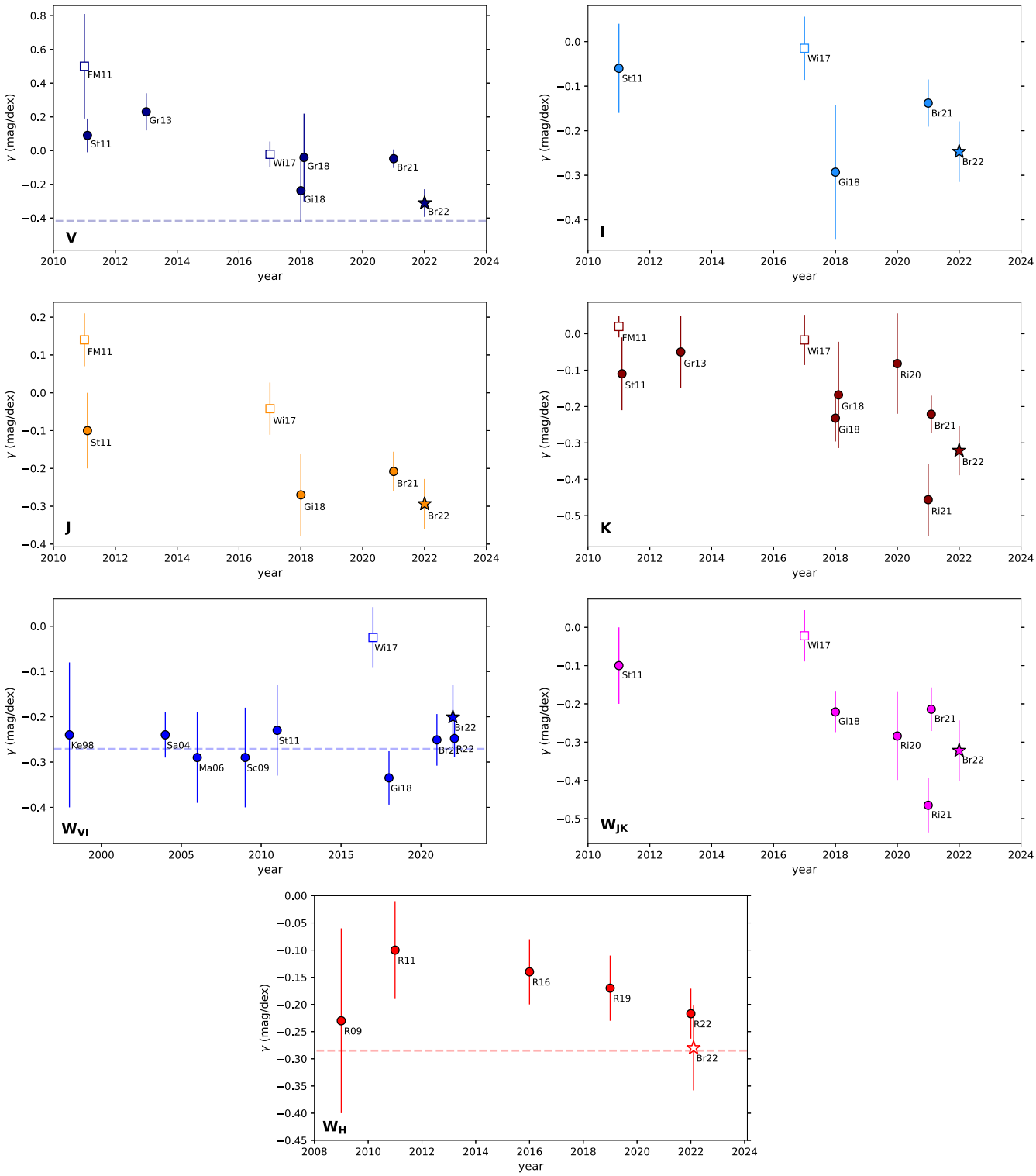

Figure 4. Evolution of the metallicity term γ in different filters over time. Open squares indicate the studies in which we identified issues that likely affect the accuracy of the corresponding γ values. The open star in the bottom panel indicates that the present work in W_H does not include HST photometry for the SMC sample. **References**: (Ke98) Kennicutt & Stetson (1998), (Sa04) Sakai et al. (2004), (Ma06) Macri et al. (2006), (Sc09) Scowcroft et al. (2009), (R09) Riess et al. (2009), (FM11) Freedman & Madore (2011), (St11) Storm et al. (2011a), (R11) Riess et al. (2011), (Gr13) Groenewegen (2013), (R16) Riess et al. (2016), (Wi17) Wielgórski et al. (2017), (Gi18) Gieren et al. (2018), (Gr18) Groenewegen (2018), (R19) Riess et al. (2019), (Ri20) Ripepi et al. (2020), (Ri21) Ripepi et al. (2021), (R22) Riess et al. (2022), (Br21) Breuval et al. (2021), (Br22) present work. The dashed colored line represents the prediction of γ from Anderson et al. (2016) using Geneva evolution models including the effects of rotation.

Thus, the distances to the Cepheids in outer regions of the SMC may differ significantly from the mean SMC distance modeled from the DEBs, perhaps due to the structures of the Magellanic stream (Nidever et al. 2008).

We can reproduce the findings of Wielgórski et al. (2017) by neglecting the correction for the SMC geometry and when considering all SMC Cepheids ($R > 2°$) for which we obtain the same low metallicity dependence as Wielgórski et al. (2017).

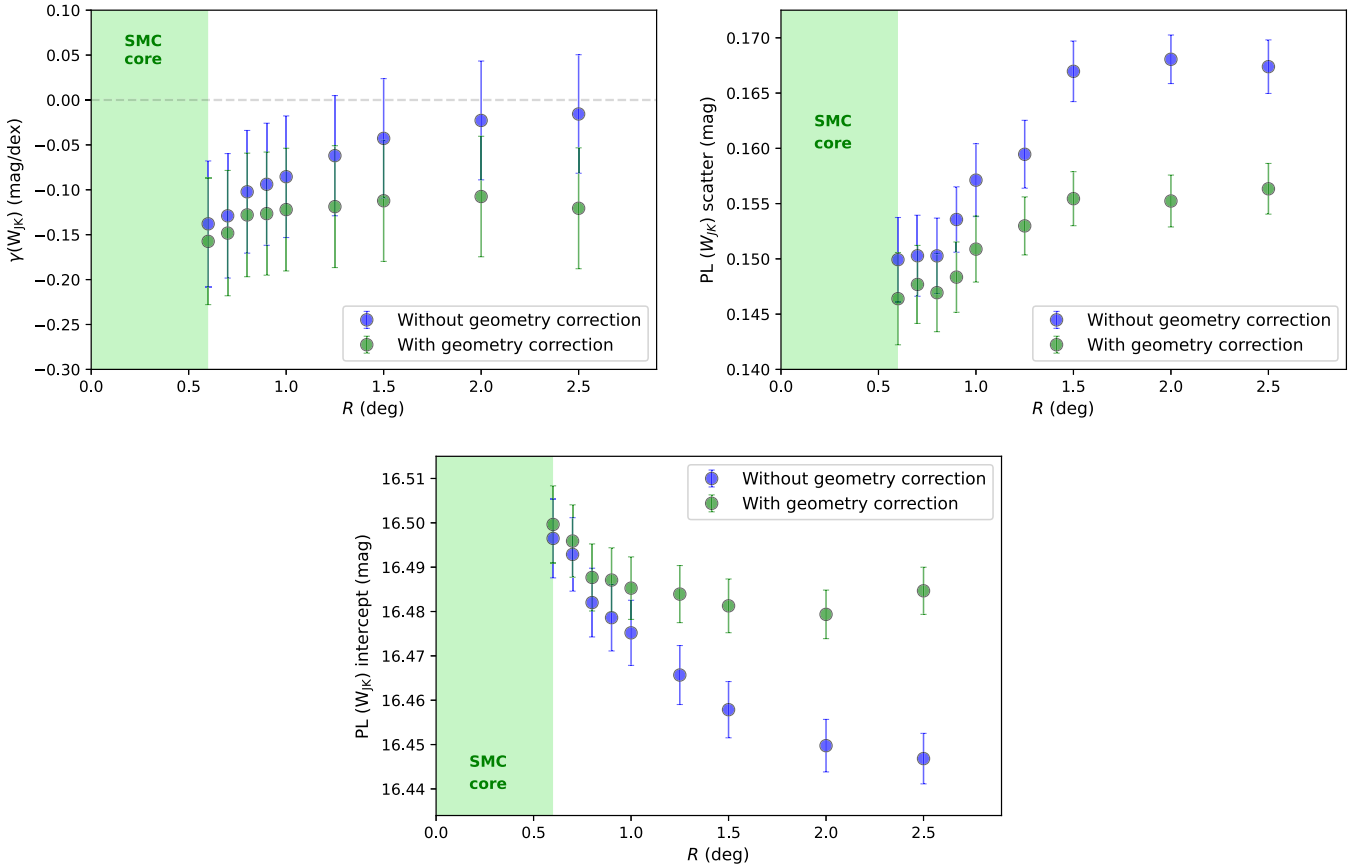

Figure 5. Metallicity effect (γ; top left panel), PL scatter (top right panel), and PL intercept (bottom panel) in the W_{JK} band as a function of the radius of the SMC region considered. The values are based on the data set and method adopted by Wielgórski et al. (2017). Blue points are the values found in the same conditions as Wielgórski et al. (2017), and green points represent the values obtained after correcting for the SMC geometry (Graczyk et al. 2020).

However, the γ term becomes more negative when we retain Cepheids in a smaller region, and it reaches -0.150 mag dex^{-1} for $R < 0.^{\circ}6$. When the geometry of the SMC is included in apparent magnitudes, γ is particularly stable between $R = 0.^{\circ}6$ and 2° with a value of -0.150 mag dex^{-1}. This demonstrates that the very low metallicity effect found by Wielgórski et al. (2017) is likely due to unaccounted for differences in depth; limiting their analysis to a narrower region of the SMC and applying geometry corrections would yield a γ value no longer consistent with zero. This issue was already mentioned by Gieren et al. (2018). We note that the γ values described in this section and represented in Figure 5 differ from our results listed in Table 5, since they are based on the data and method from Wielgórski et al. (2017; i.e., LMC and SMC samples only).

Owens et al. (2022, hereafter OW22) compared Cepheids and geometric distances in the MW, LMC, and SMC and claimed poor agreement, attributing this to an error in the Gaia EDR3 parallaxes and proposing a large, positive Gaia parallax offset coupled with no Cepheid metallicity term (including for the commonly found one in W_{VI}), with the consequence of a shorter Cepheid distance scale and higher Hubble constant.[8]

There are numerous important differences in the data used by OW22 and ours; OW22 largely employs older and less consistently calibrated photometry and reddening estimates[9] and a much smaller sample of MW Cepheids in the optical, 37 versus the ∼150 used here. We also use specific high-quality, space-based Cepheid photometry from HST (MW, LMC) and Gaia (MW, LMC, SMC) not used in the OW22 study. It is beyond the scope of this study to analyze the impacts of the older and newer data samples, but we would not be surprised if they produce systematic differences at the few hundredths of a magnitude level relevant to the ∼0.1 mag effects of metallicity (e.g., between the LMC and SMC).

However, we identify two specific differences in the measurements between the LMC and SMC that appear to impact the OW22 calculation and are independent of Gaia and its calibration. The difference in distance between the DEBs in the LMC and SMC is given by Graczyk et al. (2020) as 0.500 ± 0.017 mag. The excess difference we find between the

[8] The +18 μas Gaia offset for bright objects proposed by OW22 conflicts with the ∼−15 μas mean of the measurements external to Gaia as summarized by Lindegren et al. (2021) and shown in Figure 1 by Li et al. (2022). This offset also makes the Cepheids in OW22 fainter by 0.074 mag and the Clouds closer by that amount and raises the local Hubble constant and its present tension by ∼3.5% without a metallicity term. In contrast, the metallicity term between the Clouds and MW presented here rather than a large positive Gaia offset provides consistency between the Gaia and DEB distances, as they are the same size and direction.

[9] For the MW NIR, the OW22 photometry is from Welch et al. (1984), Laney & Stobie (1992), and Barnes et al. (1997), whereas ours is from Monson & Pierce (2011), with the latter having twice as many Cepheids and better calibration. For MW reddenings, OW22 used the Fernie et al. (1995) database, a literature compilation of photoelectric photometry from uncommon bandpasses with a mean era of the 1980s, and the Cardelli et al. (1989) reddening law, products that have not benefited from the modern wide-field studies from Pan-STARRS and SDSS like Bayestar (Green et al. 2019). For the LMC NIR data, OW22 used 92 Cepheids from Persson et al. (2004), whereas this study augments that with >750 Cepheids from Macri et al. (2015). For the SMC NIR data, OW22 used data from Welch et al. (1984), Laney & Stobie (1986), and Storm et al. (2004), whereas we use a larger sample from Kato et al. (2007) and Ripepi et al. (2016).

SMC core and the LMC (Table 4) averaged across all bands is 0.08 mag (SMC Cepheids are net fainter). For the 0.34 dex difference in Cloud metallicity, the metallicity term is then ∼0.24 mag per dex. Authors OW22 gave a best differential distance of 0.511 ± 0.056 mag for an excess of 0.01 mag, 0.07 mag smaller than found here and implying a negligible metallicity term in all bands (including the Wesenheit band, W_{VI}, which has generally been found to be -0.2 mag dex^{-1}; see Table 1). However, as Figure 5 shows, the depth of the SMC at large radii adds dispersion and reduces the apparent distance. The OW22 study uses SMC data from Scowcroft et al. (2016) with a radius from the core of up to 2°. Scowcroft et al. (2016) also noted a large spatial dependence in Cepheid distance across the greater region of the SMC. The combination of correcting for the geometry (of 0.03 mag, given but not applied in OW22) and limiting to the core (<0.°6 here) accounts for 0.06 mag of the 0.07 mag difference with our study and thus the difference between a moderate or negligible metallicity term in all bands. The known depth of the SMC and the observed reduction in the Cepheid PL scatter by correcting for the DEB-based geometry and by limiting to the core where most of the DEBs are found, yields a more accurate result. An additional 25% increase in the metallicity term between the LMC and SMC comes from the decrease in the metallicity difference between the Clouds between Romaniello et al. (2008) used by OW22 and Romaniello et al. (2022) used here.

5.6. Comparison between Empirical Estimates and Theoretical Predictions

While empirical estimates of the metallicity term of the PL relation have become more precise due to better parallaxes (Gaia Collaboration et al. 2021), reddening estimates, Cepheid photometry, and knowledge of Cloud geometry, they may appear to conflict with earlier predictions from the theory based on nonlinear convecting models (Bono et al. 1999, 2008; Caputo et al. 2000; Marconi et al. 2005). These studies suggested a positive sign for the γ term, meaning that metal-rich Cepheids would be fainter. On the other hand, Anderson et al. (2016) recently performed a pulsation instability analysis of the linear Geneva stellar evolution models by Georgy et al. (2013) that included the effects of rotation. They predicted the PL relation in V, H, W_{VI}, and W_H for three different metal abundances ($Z = 0.014$, 0.006, and 0.002, selected to match the MW, LMC, and SMC Cepheid mean metallicity, respectively) and separately on the red and blue edges of the instability strip. We averaged the PL intercepts β listed in Table 2 of Anderson et al. (2016) on both edges for the second and third crossing of the instability strip and represented them with [Fe/H] in Figure 6. We find that the variation of these intercepts with [Fe/H] yields a negative metallicity effect of $\gamma \sim -0.27$ to -0.42 mag dex^{-1} across the optical and NIR, consistent with our present results. Similarly, De Somma et al. (2022) presented an extended set of nonlinear convective pulsation models for different metallicity values and also concluded with a negative metallicity term in different Wesenheit indices (see Table 1), in agreement with Anderson et al. (2016); these two theoretical studies best fit our observational data. Additionally, the Anderson et al. (2016) models reproduce particularly well the observed boundaries of the instability strip (Groenewegen 2020). While additional theoretical studies are warranted, the agreement found here is quite promising.

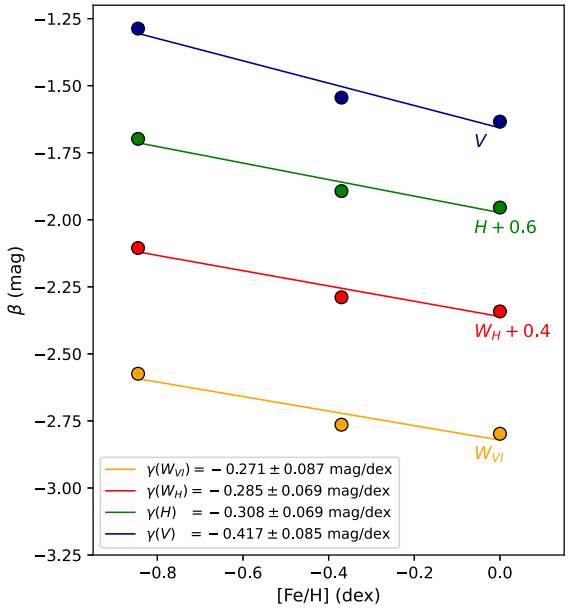

Figure 6. Metallicity effect predicted by Anderson et al. (2016) using the Geneva evolution models including rotation.

6. Conclusions and Perspectives

The results by B21 suggested a possible dependence of γ with wavelength but were based on only five filters. To explore this question, we extended the wavelength range by including new MIR (Spitzer) and optical (Gaia) bands. We were able to take this analysis one step further by improving the technique and updating the data wherever possible. All of the improvements included in this study are listed in Table 6 and compared with the previous B21 paper. We note that the uncertainties on the γ terms presented in this paper are not significantly smaller compared with previous analysis, despite the several improvements included; this is because we now include the uncertainties on the reddening law and the R_V values, which were not considered previously.

We report values of the metallicity effect on the Cepheid PL relation in 10 filters from 0.5 to 4.5 μm and in five Wesenheit indices, including the HST-based Wesenheit index W_H used for the SH0ES distance ladder (Riess et al. 2022). We obtain a negative γ term in all bands, meaning that metal-rich Cepheids are brighter than metal-poor ones, in agreement with all recent empirical studies. We find a globally uniform value of γ of about -0.28 mag dex^{-1} from optical to MIR filters, showing that the main influence of metallicity on Cepheids is in their brightness rather than color.

While our results are largely consistent with recent measurements, we track differences in two studies (Wielgórski et al. 2017; Owens et al. 2022) that employ the SMC to a depth effect. Correcting for the geometry and limiting the radius to the SMC core is shown to narrow the distance range, resulting in a sample ensured to be at the same distance as the DEBs that also produces a metallicity term on the same trend line as seen between the MW and LMC.

Comparing Cepheids over a sufficiently large metallicity range still requires combining different samples of Cepheids located in several galaxies having different distances, photometric systems, dust distribution, and properties (e.g., reddening law), which implies large systematic uncertainties. In the near future, it should be possible to reduce the impact of

Table 6
Main Improvements and Updates between B21 and the Present Analysis

	B21	This Work
Filters	V, I, J, H, K	V, I, J, H, K Gaia G, BP, RP Spitzer [3.6], [4.5]
Wesenheit indices	W_{VI}, W_{JK}	W_{VI}, W_{JK} W_{VK}, W_H (HST), W_G (Gaia)
Reddening law	A_λ/A_V from Cardelli et al. (1989)	A_λ/A_V from Fitzpatrick (1999) + uncertainties on A_λ/A_V values + uncertainties on R_V (3.1 ± 0.1)
Gaia EDR3 parallax ZP	Lindegren et al. (2021) $\varpi = \varpi_0 - \mathrm{ZP}_{L21}$	Lindegren et al. (2021) $\varpi = \varpi_0 - (\mathrm{ZP}_{L21} + 0.014\ \mu\mathrm{as})$
LMC metallicity	$[\mathrm{Fe/H}] = -0.34 \pm 0.06$ dex (Gieren et al. 2018)	$[\mathrm{Fe/H}] = -0.407 \pm 0.020$ dex (Romaniello et al. 2022)
Reddening for MW Cepheids	A13, K03, LC07, S07, A12, F95	(a) Bayestar dust map (Green et al. 2019) (b) Period–color relation (Riess et al. 2022) (c) SPIPS method (Trahin et al. 2021)
Reddening for LMC and SMC Cepheids	Górski et al. (2020) reddening maps	Skowron et al. (2021) reddening maps
V, I photometry for LMC Cepheids	OGLE-IV (Soszyński et al. 2015)	OGLE-IV (Soszyński et al. 2015) + Shallow Survey (Ulaczyk et al. 2013)
G, BP, RP photometry	Gaia DR2 light curves (Clementini et al. 2019)	Gaia EDR3 light curves (Ripepi et al. 2022c)

References: (A13) Anderson et al. (2013), (K08) Kovtyukh et al. (2008), (LC07) Laney & Caldwell (2007), (S07) Sziládi et al. (2007), (A12) Acharova et al. (2012), (F95) Fernie et al. (1995).

these systematics and increase the precision of the γ term thanks to the fourth Gaia data release. Ideally, these new distance measurements will have to be combined with consistent metallicity estimates of all MW Cepheids obtained in a single system, spanning a wide range of abundances. In this sense, improvements are also expected from the use of recently published (Ripepi et al. 2021; Romaniello et al. 2022; da Silva et al. 2022) and upcoming abundance catalogs for MW, LMC, and SMC Cepheids, which should again help to calibrate the metallicity effect with better accuracy.

We thank the referee for the constructive report that helped to improve the present paper. L.B. is grateful to C. A. L. Bailer-Jones, F. Arénou, B. Trahin, L. M. Macri, S. Casertano, and A. Mérand for inspiring discussions that helped to improve the present work. We thank L. M. Macri for providing the photometric transformations to the 2MASS system. We are grateful to V. Ripepi for providing the full list of reclassified Cepheids with Gaia DR3. The research leading to these results has received funding from the European Research Council (ERC) under the European Union's Horizon 2020 research and innovation program (projects CepBin, grant agreement 695099, and UniverScale, grant agreement 951549). This work has made use of data from the European Space Agency (ESA) mission Gaia (https://www.cosmos.esa.int/gaia), processed by the Gaia Data Processing and Analysis Consortium (DPAC; https://www.cosmos.esa.int/web/gaia/dpac/consortium). Funding for the DPAC has been provided by national institutions, in particular the institutions participating in the Gaia Multilateral Agreement. The results presented in this paper benefited from discussions with the International Space Science Institute (ISSI) team led by G. Clementini.[10] This research has made use of Astropy, a community-developed core Python package for astronomy (Astropy Collaboration et al. 2018). We used the SIMBAD and VIZIER databases and catalog access tool at the CDS, Strasbourg (France), and NASA's Astrophysics Data System Bibliographic Services. This research has made use of the SVO Filter Profile Service.[11] Some of the data presented in this paper were obtained from the Mikulski Archive for Space Telescopes (MAST) at the Space Telescope Science Institute. The specific observations analyzed can be accessed via doi:10.17909/t9-my41-h234 and doi:10.17909/t9-2gmg-xc49.

Appendix

Figure 7 shows the metallicity effect γ as a function of the inverse of wavelength, in the case where the mean metallicity of SMC Cepheids would be −0.90 dex (see discussion in Section 5.4).

[10] https://www.issibern.ch/teams/shot/
[11] http://svo2.cab.inta-csic.es/theory/fps/

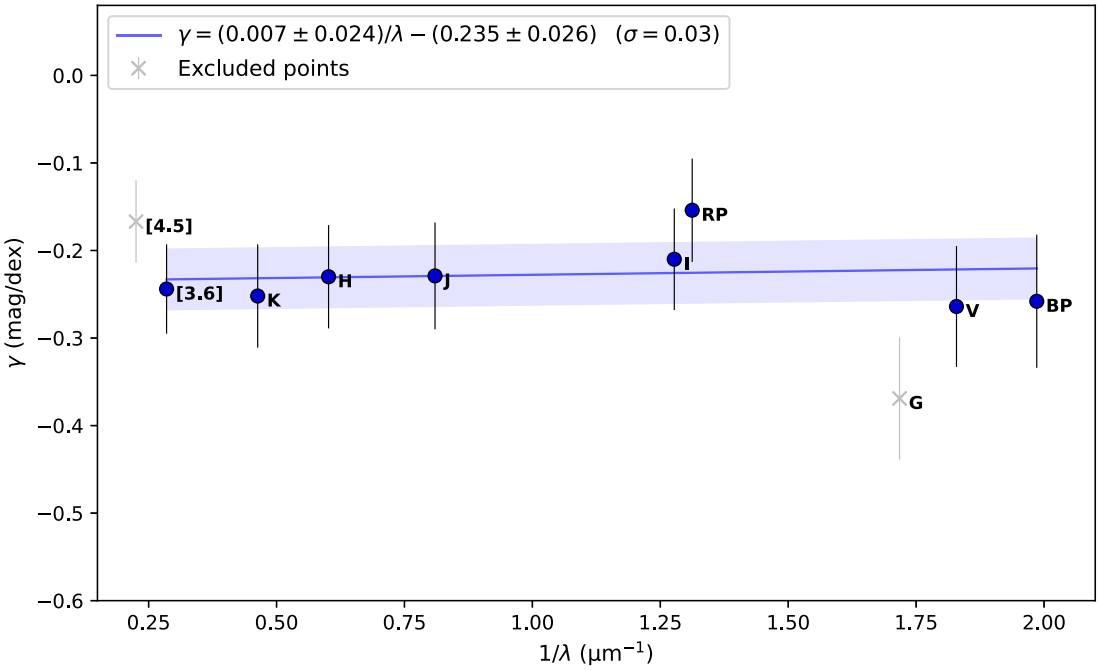

Figure 7. Metallicity effect (γ) as a function of the inverse of wavelength ($1/\lambda$) in the hypothesis of a more metal-poor SMC sample of -0.90 ± 0.05 dex (see discussion in Section 5.4).

ORCID iDs

Louise Breuval https://orcid.org/0000-0003-3889-7709
Adam G. Riess https://orcid.org/0000-0002-6124-1196
Pierre Kervella https://orcid.org/0000-0003-0626-1749
Richard I. Anderson https://orcid.org/0000-0001-8089-4419
Martino Romaniello https://orcid.org/0000-0002-5527-6317

References

Acharova, I. A., Mishurov, Y. N., & Kovtyukh, V. V. 2012, MNRAS, 420, 1590
Anderson, R. I., Eyer, L., & Mowlavi, N. 2013, MNRAS, 434, 2238
Anderson, R. I., Saio, H., Ekström, S., Georgy, C., & Meynet, G. 2016, A&A, 591, A8
Astropy Collaboration, Price-Whelan, A. M., & Sipőcz, B. M. 2018, AJ, 156, 123
Bailer-Jones, C. A. L., Rybizki, J., Fouesneau, M., Demleitner, M., & Andrae, R. 2021, AJ, 161, 147
Barnes, T. G. I., Fernley, J. A., Frueh, M. L., et al. 1997, PASP, 109, 645
Berdnikov, L. N. 2008, yCat, 2285, 0
Bono, G., Caputo, F., Castellani, V., & Marconi, M. 1999, ApJ, 512, 711
Bono, G., Caputo, F., Fiorentino, G., Marconi, M., & Musella, I. 2008, ApJ, 684, 102
Breuval, L., Kervella, P., Wielgórski, P., et al. 2021, ApJ, 913, 38
Caputo, F., Marconi, M., Musella, I., & Santolamazza, P. 2000, A&A, 359, 1059
Cardelli, J. A., Clayton, G. C., & Mathis, J. S. 1989, ApJ, 345, 245
Clementini, G., Ripepi, V., Molinaro, R., et al. 2019, A&A, 622, A60
Cruz Reyes, M., & Anderson, R. I. 2022, arXiv:2208.09403
da Silva, R., Crestani, J., Bono, G., et al. 2022, A&A, 661, A104
De Somma, G., Marconi, M., Molinaro, R., et al. 2022, ApJS, 262, 25
Di Valentino, E., Mena, O., Pan, S., et al. 2021, CQGra, 38, 153001
Efron, B., & Tibshirani, R. 1986, Statist. Sci., 1, 54
Fernie, J. D., Evans, N. R., Beattie, B., & Seager, S. 1995, IBVS, 4148, 1
Fitzpatrick, E. L. 1999, PASP, 111, 63
Fitzpatrick, E. L., Massa, D., Gordon, K. D., Bohlin, R., & Clayton, G. C. 2019, ApJ, 886, 108
Freedman, W. L., & Madore, B. F. 2011, ApJ, 734, 46
Freedman, W. L., Madore, B. F., Gibson, B. K., et al. 2001, ApJ, 553, 47
Freedman, W. L., Madore, B. F., Scowcroft, V., et al. 2011, AJ, 142, 192
Gaia Collaboration, Brown, A. G. A., Vallenari, A., et al. 2021, A&A, 649, A1
Gaia Collaboration, Prusti, T., de Bruijne, J. H. J., et al. 2016, A&A, 595, A1
Gaia Collaboration, Vallenari, A., Brown, A. G. A., et al. 2022, arXiv:2208.00211
Genovali, K., Lemasle, B., Bono, G., et al. 2014, A&A, 566, A37
Genovali, K., Lemasle, B., da Silva, R., et al. 2015, A&A, 580, A17
Georgy, C., Ekström, S., Granada, A., et al. 2013, A&A, 553, A24
Gieren, W., Storm, J., Konorski, P., et al. 2018, A&A, 620, A99
González-Fernández, C., Hodgkin, S. T., Irwin, M. J., et al. 2018, MNRAS, 474, 5459
Gordon, K. D., Clayton, G. C., Misselt, K. A., Landolt, A. U., & Wolff, M. J. 2003, ApJ, 594, 279
Górski, M., Zgirski, B., Pietrzyński, G., et al. 2020, ApJ, 889, 179
Graczyk, D., Pietrzyński, G., Thompson, I. B., et al. 2014, ApJ, 780, 59
Graczyk, D., Pietrzyński, G., Thompson, I. B., et al. 2020, ApJ, 904, 13
Green, G. M., Schlafly, E., Zucker, C., Speagle, J. S., & Finkbeiner, D. 2019, ApJ, 887, 93
Groenewegen, M. A. T. 2013, A&A, 550, A70
Groenewegen, M. A. T. 2018, A&A, 619, A8
Groenewegen, M. A. T. 2020, A&A, 635, A33
Indebetouw, R., Mathis, J. S., Babler, B. L., et al. 2005, ApJ, 619, 931
Inno, L., Bono, G., Matsunaga, N., et al. 2016, ApJ, 832, 176
Jacyszyn-Dobrzeniecka, A. M., Skowron, D. M., Mróz, P., et al. 2016, AcA, 66, 149
Kato, D., Nagashima, C., Nagayama, T., et al. 2007, PASJ, 59, 615
Kennicutt, R. C. J., Stetson, P. B., Saha, A., et al. 1998, ApJ, 498, 181
Kovtyukh, V. V., Soubiran, C., Luck, R. E., et al. 2008, MNRAS, 389, 1336
Laney, C. D., & Caldwell, J. A. R. 2007, MNRAS, 377, 147
Laney, C. D., & Stobie, R. S. 1986, MNRAS, 222, 449
Laney, C. D., & Stobie, R. S. 1992, A&AS, 93, 93
Leavitt, H. S., & Pickering, E. C. 1912, HarCi, 173, 1
Li, S., Casertano, S., & Riess, A. G. 2022, arXiv:2202.11110
Lindegren, L., Bastian, U., Biermann, M., et al. 2021, A&A, 649, A4
Macri, L. M., Ngeow, C.-C., Kanbur, S. M., Mahzooni, S., & Smitka, M. T. 2015, AJ, 149, 117
Macri, L. M., Stanek, K. Z., Bersier, D., Greenhill, L. J., & Reid, M. J. 2006, ApJ, 652, 1133
Madore, B. F. 1982, ApJ, 253, 575
Marconi, M., Musella, I., & Fiorentino, G. 2005, ApJ, 632, 590
Marengo, M., Evans, N. R., Barmby, P., et al. 2010, ApJ, 725, 2392
Mérand, A., Kervella, P., Breitfelder, J., et al. 2015, A&A, 584, A80
Monson, A. J., Freedman, W. L., Madore, B. F., et al. 2012, ApJ, 759, 146
Monson, A. J., & Pierce, M. J. 2011, ApJS, 193, 12

Nidever, D. L., Majewski, S. R., & Butler Burton, W. 2008, ApJ, 679, 432
Owens, K. A., Freedman, W. L., Madore, B. F., & Lee, A. J. 2022, ApJ, 927, 8
Persson, S. E., Madore, B. F., Krzemiński, W., et al. 2004, AJ, 128, 2239
Pietrzyński, G., Graczyk, D., Gieren, W., et al. 2013, Natur, 495, 76
Pietrzyński, G., Graczyk, D., Gallenne, A., et al. 2019, Natur, 567, 200
Planck Collaboration, Aghanim, N., Akrami, Y., et al. 2020, A&A, 641, A6
Riess, A. G., Casertano, S., Yuan, W., et al. 2021, ApJL, 908, L6
Riess, A. G., Casertano, S., Yuan, W., Macri, L. M., & Scolnic, D. 2019, ApJ, 876, 85
Riess, A. G., Macri, L., Casertano, S., et al. 2009, ApJ, 699, 539
Riess, A. G., Macri, L., Casertano, S., et al. 2011, ApJ, 730, 119
Riess, A. G., Macri, L. M., Hoffmann, S. L., et al. 2016, ApJ, 826, 56
Riess, A. G., Yuan, W., Macri, L. M., et al. 2022, ApJL, 934, L7
Ripepi, V., Cioni, M.-R. L., Moretti, M. I., et al. 2017, MNRAS, 472, 808
Ripepi, V., Catanzaro, G., Molinaro, R., et al. 2020, A&A, 642, A230
Ripepi, V., Catanzaro, G., Molinaro, R., et al. 2021, MNRAS, 508, 4047
Ripepi, V., Catanzaro, G., Clementini, G., et al. 2022a, A&A, 659, A167
Ripepi, V., Chemin, L., Molinaro, R., et al. 2022b, MNRAS, 512, 563
Ripepi, V., Clementini, G., Molinaro, R., et al. 2022c, arXiv:2206.06212
Ripepi, V., Marconi, M., Moretti, M. I., et al. 2016, ApJS, 224, 21
Ripepi, V., Molinaro, R., Musella, I., et al. 2019, A&A, 625, A14
Romaniello, M., Primas, F., Mottini, M., et al. 2008, A&A, 488, 731
Romaniello, M., Riess, A., Mancino, S., et al. 2022, A&A, 658, A29
Sakai, S., Ferrarese, L., Kennicutt, Robert, C., & Saha, A, J. 2004, ApJ, 608, 42
Sandage, A., Tammann, G. A., & Reindl, B. 2009, A&A, 493, 471
Scowcroft, V., Bersier, D., Mould, J. R., & Wood, P. R. 2009, MNRAS, 396, 1287
Scowcroft, V., Freedman, W. L., Madore, B. F., et al. 2016, ApJ, 816, 49
Scowcroft, V., Freedman, W. L., Madore, B. F., et al. 2011, ApJ, 743, 76
Sharpee, B., Stark, M., Pritzl, B., et al. 2002, AJ, 123, 3216
Skowron, D. M., Skowron, J., Udalski, A., et al. 2021, ApJS, 252, 23
Soszyński, I., Poleski, R., Udalski, A., et al. 2010, AcA, 60, 17
Soszyński, I., Udalski, A., Szymański, M. K., et al. 2015, AcA, 65, 297
Storm, J., Carney, B. W., Gieren, W. P., et al. 2004, A&A, 415, 531
Storm, J., Gieren, W., Fouqué, P., et al. 2011a, A&A, 534, A95
Storm, J., Gieren, W., Fouqué, P., et al. 2011b, A&A, 534, A94
Subramanian, S., & Subramaniam, A. 2015, A&A, 573, A135
Sziládi, K., Vinkó, J., Poretti, E., Szabados, L., & Kun, M. 2007, A&A, 473, 579
Tammann, G. A., Reindl, B., & Sandage, A. 2011, A&A, 531, A134
Trahin, B., Breuval, L., Kervella, P., et al. 2021, A&A, 656, A102
Udalski, A., Szymanski, M., Kubiak, M., et al. 1999, AcA, 49, 201
Ulaczyk, K., Szymański, M. K., Udalski, A., et al. 2013, AcA, 63, 159
Welch, D. L., Wieland, F., McAlary, C. W., et al. 1984, ApJS, 54, 547
Wielgórski, P., Pietrzyński, G., Gieren, W., et al. 2017, ApJ, 842, 116
Zinn, J. C. 2021, AJ, 161, 214